THE JOURNAL OF PHYSICAL CHEMISTRY LETTERS
A JOURNAL OF THE AMERICAN CHEMICAL SOCIETY

pubs.acs.org/JPCL

Letter

Temperature-Dependent Low-Frequency Modes in the Active Site of Bovine Carbonic Anhydrase II Probed by 2D-IR Spectroscopy

Julian M. Schmidt-Engler, Sarah von Berg, and Jens Bredenbeck*

Cite This: *J. Phys. Chem. Lett.* 2021, 12, 7777−7782

Read Online

ACCESS | Metrics & More | Article Recommendations | Supporting Information

ABSTRACT: Enzyme catalysis achieves tremendous rate accelerations. Enzyme reaction centers provide a constraint geometry that preferentially binds an activated form of the substrate and thus lowers the energy barrier. However, this transition state picture neglects the flexibility of proteins and its role in enzymatic catalysis. Especially for proton transfer reactions, it has been suggested that motions of the protein modulate the donor−acceptor distance and prepare a tunneling-ready state. We report the detection of frequency fluctuations of an azide anion (N_3^-) bound in the active site of the protein carbonic anhydrase II, where a low-frequency mode of the protein has been proposed to facilitate proton transfer over two water molecules during the catalyzed reaction. 2D-IR spectroscopy resolves an underdamped low-frequency mode at about 1 THz (30 cm^{-1}). We find its frequency to be viscosity- and temperature-dependent and to decrease by 6 cm^{-1} between 230 and 320 K, reporting the softening of the mode's potential.

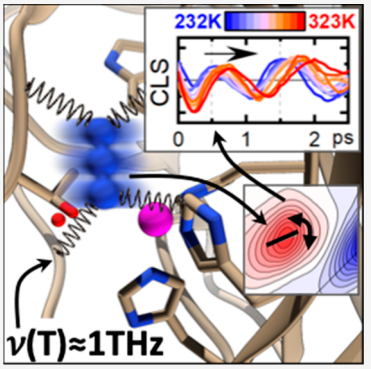

Enzymatic catalysis provides gains in turnover rate of up to 10^{20} compared to the uncatalyzed reaction.[1] Despite the work devoted during the past decades, many aspects of the underlying mechanisms are still not well understood. Biomimetic and industrial approaches largely fail to parallel the enzyme's enormous rate accelerations.[2] Our understanding mainly still relies on the transition state (TS) approach introduced by Pauling, which proposes preferential binding of the enzyme to an activated form of the substrate(s) at the TS.[3,4] In this static picture of biocatalysis, binding of the substrate releases energy, which stabilizes the transition state and thus lowers the energy barrier of the reaction.[5]

However, even in simple cases it is difficult to imagine an enzyme binding the substrate, catalyzing the reaction, and releasing the product from a single conformational state.[6] For motions on the picosecond time scale, there is a plethora of theoretical/computational[7−11] and experimental[12−14] evidence that they aid enzymatic function. Thermally activated motions that are coupled directly to the reaction coordinate have been found to have a rate promoting effect by stabilizing the TS and, furthermore, manipulating the DAD toward a tunneling-ready state. According rate promoting vibrations (RPV's) were proposed based on simulations for the enzyme lactate dehydrogenase (LDH), where a collective compressive motion of the protein is believed to facilitate tunneling processes in the active site.[11,15,16] Nevertheless, the role of dynamics for the chemical step of enzyme catalysis remains under debate.[17−21]

A protein that is also suspected to feature RPV's is carbonic anhydrase II (CAII), which catalyzes the reaction of CO_2 to HCO_3^-.[22,23] Its active site contains a zinc (Zn) ion that is coordinated by three histidine residues and an OH^- ion. After reaction with CO_2, the formed HCO_3^- is replaced by H_2O. Its complex active site dynamics have brought CAII into the focus of numerous studies using ultrafast vibrational spectroscopy.[24,25] To recover the active site, the excess proton is thought to be transferred along a bridge of two water molecules to the 8 Å away His-64.[23] Proton transfer over single bonds tends to happen via tunneling. Such cases can be identified by a large primary kinetic isotope effect (KIE), which is defined as the ratio between the proton and the deuteron rate constant. For the rate-determining step in CAII this is also the case with a KIE of 3−4.[26,27] Furthermore, the rate constant in mixtures of H_2O/D_2O depends exponentially on the D_2O content, suggesting that more than one proton is involved in the process.[28] Simulations of a reduced active site model of CAII showed a triple-proton transfer that is concerted, that is, occurs by tunneling through a single barrier. Furthermore, the simulation suggested that strong coupling to low-frequency skeletal modes of the protein activate the tunneling process.[22]

In this Letter we provide experimental evidence for low-frequency modes modulating the active site of bovine CAII (BCAII) and investigate their temperature and viscosity dependence. We employed femtosecond two-dimensional infrared (2D-IR) spectroscopy on the antisymmetric stretching mode of N_3^-. N_3^- is bound in place of the hydroxide ion to the

Received: May 6, 2021
Accepted: August 5, 2021
Published: August 10, 2021

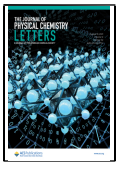

https://doi.org/10.1021/acs.jpclett.1c01453
J. Phys. Chem. Lett. 2021, 12, 7777−7782

active site's Zn as depicted in the left panel of Figure 1 and serves as strong IR probe. Because of the lack of a BCAII–N_3^-

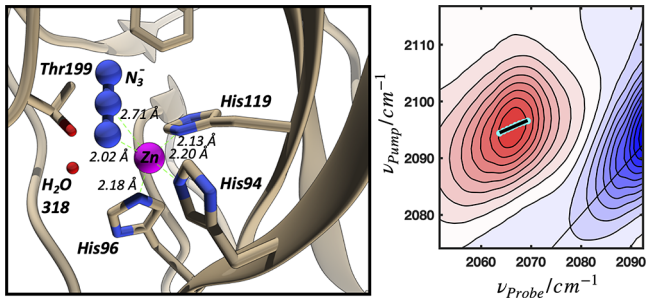

Figure 1. Left panel shows the X-ray crystal structure of HCAII (pdb: 1RAY) in a complex with N_3^-. The coordination distances to the active site Zn atom (magenta) are shown for the three involved histidine's and the N_3^- molecule. The right panel shows the 2D-IR spectrum of the antisymmetric stretching mode of N_3^- at 0.6 ps and 283 K. The maxima of the 1–2 transition are shown as cyan dots, and their linear fit, the centerline, is shown as a black bar. The diagonal of the spectrum is shown as a black line. A detailed time series of 15 2D-IR spectra (for each temperature 2D-IR spectra at 65 delays were collected) for N_3^- in BCAII at 283 K including the CLS analysis are presented in Figure S2.

complex structure, the active site of human CAII (HCAII) with N_3^- is shown (pdb: 1RAY[29]), which has 99.6% structural overlap[30] with BCAII (pdb: 1V9E;[31] superimposed structures are presented in Figure S1). Buried in the active site, N_3^- is shielded from the thermal noise of the solvent and therefore can detect motions at the active site.[32] Such direct observation of low-frequency active site modes has been so far only reported for the protein formate dehydrogenase (FDH) by Cheatum and co-workers.[32−34] In catalase, coherent oscillations in the pump–probe transients of heme-bound NO have been assigned to anharmonic coupling of the NO stretch to enzyme low-frequency modes in a similar wavenumber range.[35]

The 2D-IR experiment infers local dynamics in the proximity of an IR probe oscillator by measuring the frequency correlation between its excitation frequency ν_{pump} and detection frequency ν_{probe} as a function of the waiting time (T_w). The frequency of an oscillator is sensitive to its chemical surrounding (e.g., protein and buffer);[36] hence, monitoring the frequency evolution directly reports on the surroundings' dynamics. A high level of frequency correlation is found when the frequency of an oscillator is detected shortly after excitation, as its environment had no time to evolve. Here ν_{pump} equals ν_{probe} for the underlying vibrations; therefore, the 2D line shape is elongated along the diagonal of the spectrum. Driven by thermally activated motions, the environment changes. This so-called spectral diffusion diminishes the correlation to the initial frequency over time and thus reports directly on structural fluctuations in the active site. With disappearing correlation, the 2D line shape becomes more circular. Figure 1 (right panel) displays a 2D-IR spectrum of the antisymmetric stretching mode of N_3^- bound to the active site of BCAII. To quantify the change in line shape, we employ the inverse (iv) centerline slope (CLS) method.[37,38] This line shape analysis technique was chosen to minimize the effects of the presence of subensembles, which cause asymmetry of N_3^-'s FTIR spectra (see Figures S5D and S6B), and curvature of the CLS and ivCLS of the 2D-IR spectra (for a comparison of these techniques see Figure S9). To focus the analysis on the main subensemble, we used the ivCLS of the 1–2 transition, as the ivCLS results in a higher density of data points compared to the CLS, allowing to zoom in on the band center, and the 1–2 transition suffers less from a curved ivCLS (Figure S9). The centerline slope, ranging between 1 and 0, is marked by cyan dots, and the corresponding linear regression from which the slope is obtained is shown as a black bar. The slope as a function of the waiting time T_w is directly proportional to the normalized frequency–frequency correlation function (FFCF) of N_3^-.[37] Typically, the CLS decay can be modeled by an exponential or a sum of exponentials of the form

$$\mathrm{CLS}(T_w) = \sum_{i=0}^{n} \Delta_i^2 e^{-T_w/\tau_i}$$

where Δ^2 is the amplitude and τ the time constant of the exponential fit.

For free N_3^- in buffer we indeed find that the frequency correlation decays monoexponentially with a time constant of 3.66 ps (Figure 2, top panel). Here, the thermally activated

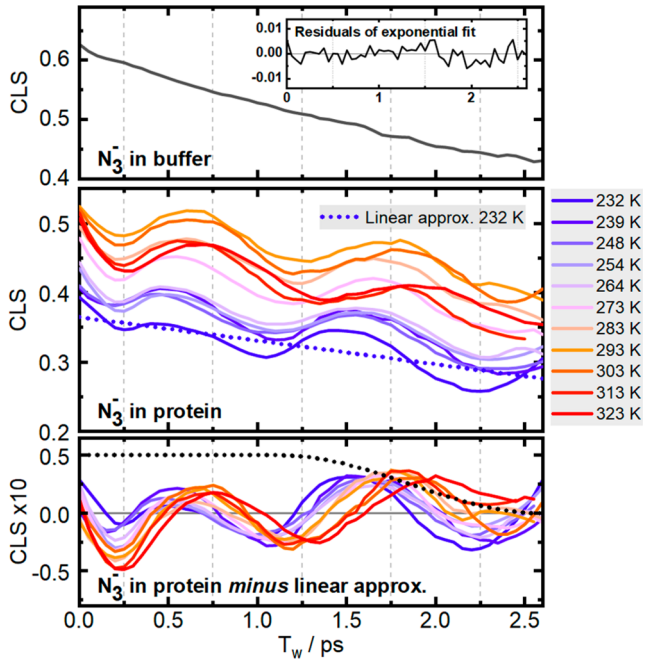

Figure 2. Top panel shows the CLS decay of N_3^- in buffer at 293 K. A monoexponential fit (R^2 = 0.99) yielded a time constant of 3.66 ps. The residuals of the fit are shown as inset to the data. The center panel shows the raw CLS data for N_3^- in BCAII at all measured temperatures (solid lines). The subtracted linear baseline is shown exemplary for the 232 K data point as a dotted blue line. The bottom panel shows the CLS data after subtraction of a linear approximation of the overall exponential CLS decay. The window function (tapered cosine) used for Fourier processing is shown as a dotted black line.

reorganization of mobile water molecules around the oscillator is observed, which affects its frequency over time. There is furthermore no trace of systematic deviations from the exponential correlation decay as the residuals (see the inset) are small and appear random.

For N_3^- in the active site of BCAII the CLS decay slows down slightly (Figure 2, center panel) compared to the free N_3^- in buffer (Figure 2, top panel). This is not surprising as the protein environment at the active site is expected to evolve slower than the solvation shell of free N_3^-. Much more

https://doi.org/10.1021/acs.jpclett.1c01453
J. Phys. Chem. Lett. 2021, 12, 7777−7782

strikingly, however, the CLS of N_3^- in the active site cannot be modeled by exponentials, in contrast to the free N_3^-, but includes an underdamped oscillation with a period of ≈1 ps (1 THz, 33 cm^{-1}), showing that frequency correlation is cyclically regained.

Figure 3 illustrates how periodic change of the environment of an IR probe, for example, by a protein low-frequency mode,

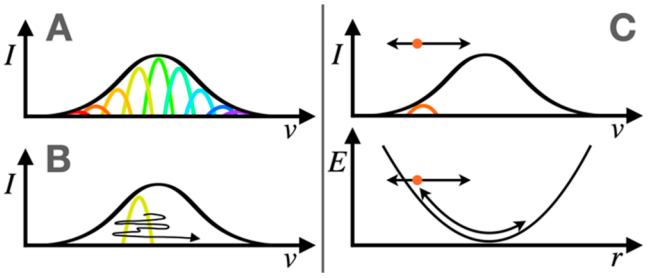

Figure 3. Schematic illustration of the correlation between the frequency of a population in the ensemble and the spatial coordinate of the environment of N_3^- moving in a harmonic potential (see text for further explanation).

leads to such oscillations in the CLS instead of the usual exponential time dependence. Figure 3A shows an absorption band (e.g., of N_3^-) which is inhomogeneously broadened by different molecular environments. After a subensemble of N_3^- *in buffer* is excited in a frequency-selective fashion, for example, the yellow band, thermally activated movements drive the reorientation of water molecules in randomized fashion (Figure 3B), leading to a loss of frequency correlation as a function of T_w. In the usual case the FFCF and thus the CLS decay exponentially due to this randomization of the environment. Figure 3C shows the situation where the frequency ν of the probe is correlated to the coordinate r of a low-frequency mode of the protein that modulates the environment of the probe. Also here, subensembles of probe oscillators (e.g., the orange band) are excited in the 2D-IR experiment. Instead of the frequency being randomized as in Figure 3B, the probe oscillators return to the same frequency with each period of the low-frequency mode. This leads to a recovery of frequency correlation, being diminished over time by dephasing of the low-frequency mode and motion along other coordinates. As pointed out by Pagano et al., oscillations of the FFCF[32] could alternatively be caused by coherent excitation of a low-frequency mode being anharmonically coupled to the excited high-frequency mode as shown by Elsaesser et al.[39] However, in such case an oscillating wave packet is created that gives rise to an intensity beating between the coupled transitions.[32,39] This effect can be ruled out here, as the spectral intensity of the N_3^- transition decays strictly exponentially (see Figure S3).

To characterize the low-frequency modes in the active site of BCAII, a time series of 2D-IR spectra were collected in the temperature range 232−323 K, in cryogenic buffer containing 66 wt % glycerol (Figure 2). Inspection of the CLS's oscillatory component, which we isolated by subtraction of a linear approximation of the overall exponential CLS decay (Figure 2, bottom panel), reveals that the period of the oscillation prolongs with rising temperature, hence lowering its frequency. A contour plot of the isolated oscillatory component (according to Figure 2, lower panel) including the extrema of each data set is presented in Figure 4A. To determine the frequency for each data set, we performed a spectral analysis using Fourier transformation (FT). The resulting spectra, shown in Figure 4B, contain the frequencies of the protein motions sensed at the active site by N_3^-. Throughout all probed temperatures one prominent feature that shifts from 33 cm^{-1} at 232 K to 27 cm^{-1} at 323 K was found. The chosen sampling interval of 50 fs ensures sampling of frequencies up to 333.6 cm^{-1}. Nevertheless, no feature at higher wavenumber than 50 cm^{-1} is shared consistently among the data. On the low wavenumber end a shoulder band is visible at around 12 cm^{-1}, which is, however, below the frequency resolution of the experiment (13.4 cm^{-1}). Therefore, we focus on the main, higher wavenumber, feature.

The frequency analysis (Figure 4C) reveals an approximately linear decline in oscillation frequency of the low-frequency mode in the temperature range 264−323 K. Aside from the temperature also the dynamic viscosity of the water−glycerol solution significantly changes in that temperature range from 92.2 to 5.0 cP. The dynamic viscosity of the cryogenic buffer as a function of the temperature in the probed range 232−323 K is shown in Figure S4. To investigate the interplay of temperature and viscosity effects onto the observed low-frequency mode, 2D-IR time series in aqueous buffer (i.e., in buffer without added glycerol) were collected at 281 and 318 K (Figure 4C). CD and FTIR spectra of BCAII−N_3^- in both buffers (Figure S5) showed that besides increasing the melting

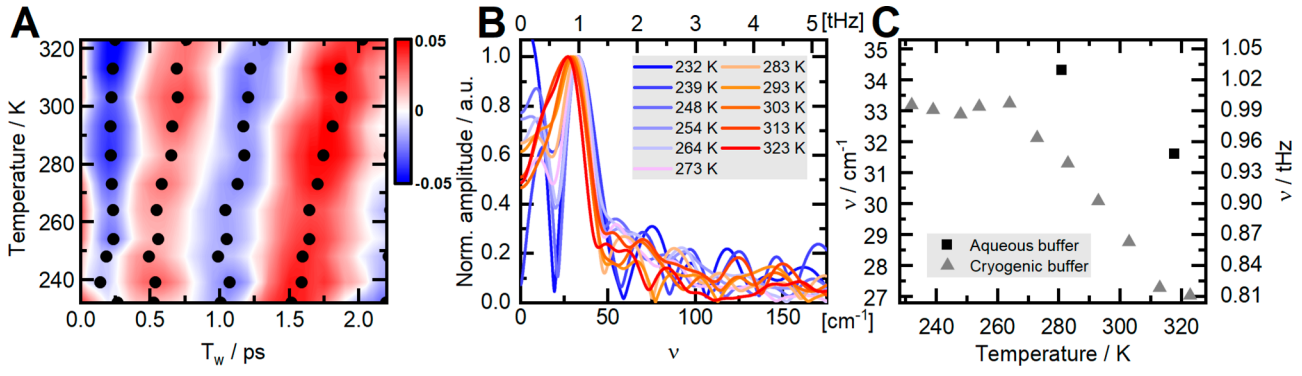

Figure 4. (A) Contour plot of the isolated oscillatory CLS part presented in the bottom panel of Figure 2 as a function of the temperature. The extrema at each temperature are shown as dots. (B) Power spectrum (normalized) of the Fourier transformations (FTs) of the oscillatory component. (C) Frequencies obtained by Fourier analysis of data collected in cryogenic buffer and aqueous buffer are shown in gray and black, respectively.

https://doi.org/10.1021/acs.jpclett.1c01453
J. Phys. Chem. Lett. 2021, 12, 7777−7782

temperature, the addition of glycerol to the buffer neither affected secondary structure content, as judged by CD spectroscopy, nor changed the local environment of N_3^- in the active site significantly, as judged by FTIR spectroscopy. Aqueous buffer is overall significantly less viscous and the viscosity less temperature dependent (1.4 cP at 281 K and 0.6 cP at 318 K) than in the cryogenic buffer. At these decreased viscosities we find about 10% higher frequencies as compared to measurements in cryogenic buffer. However, also in aqueous buffer a similar decrease in frequency with temperature is found. This shows that the impact of viscosity in that temperature range, albeit clearly influencing the observed frequency, as seen by the frequency offset of the data acquired in aqueous buffer, seems to be overcompensated by the temperature effect. With higher temperature the potential of the observed low-frequency mode apparently softens, thus lowering the oscillation frequency, as the protein explores more anharmonic regions of the potential.[40] Softening of delocalized protein modes in this frequency range was also found upon ligand binding for the protein dihydrofolate reductase (DHFR).[41]

For temperatures below 264 K, however, we observe a regime change as the frequency of the low-frequency mode barely changes. In this temperature range we find that the viscosity increases tremendously from 92.2 cP at 264 K to 3062.7 cP at 232 K (Figure S4). This finding might suggest that below 264 K the viscosity, that is, a property of the protein's environment, plays an increasing role for the dynamics of the protein as compared to the temperature-induced mode softening. That is, below 264 K the temperature-dependent increase of frequency is compensated by the frequency-decreasing effect of higher viscosity. To investigate the dynamics of the surrounding buffer, we evaluated the free N_3^- species, that is, not bound to the protein (Figure S6), that lies within the same spectral window. Over the temperature range 232−323 K we evaluated the central wavenumber of the absorption (Figures S6 and S7A), the vibrational lifetime (τ_{Vib}; Figure S7B), which directly reports on changes in the efficiency of vibrational energy relaxation, and the pure-dephasing time T_2^* (Figure S7C), which expresses the amount of ultrafast (subpicosecond) fluctuations around the probe oscillator. These additional observables hint a change in dynamics around 264 K for the free N_3^- species (Figure S7). For the bound N_3^- species, however, the temperature dependence of the central wavenumber is much less pronounced, and vibrational lifetime and pure dephasing time are almost temperature independent, confirming that the active site is isolated from the solvent. The observations that the low-frequency mode is viscosity dependent and its frequency has a similar temperature dependence as the above-mentioned parameters of the solvent exposed free N_3^- species (Figure S7) suggest that the low-frequency mode is delocalized and involves solvent-exposed parts of the protein.

Using 2D-IR spectroscopy, we were able to detect oscillations in the vibrational frequency of a small reporter molecule in the active site of BCAII. We attribute these oscillations to protein low-frequency modes in the environment of the Zn reaction center in the 1 THz range. On the path toward a generalized theory of rate acceleration achieved in biocatalysis, the role of protein motion gained momentum as it has been described as the "missing link".[2] In CAII's active site, collective motions were proposed to play a key role in proton tunneling along a water wire.[22] Using the CLS methodology, we directly observe an underdamped collective motion of BCAII that is likely to be delocalized along the protein, as indicated by the viscosity dependence. Furthermore, we observe a strong temperature dependence of this low-frequency mode between 27 and 33 cm^{-1}, which we attribute to softening of the mode's potential. It remains a subject for future studies if the mode is of any relevance for the function of the protein and how it relates to the low-frequency modes that have been proposed to couple to the reaction coordinate. The question if the observed mode in BCAII's active site is indeed related to DAD sampling during preparation of a tunneling-ready state in the proton transfer process should be addressed by MD simulations and theoretical spectroscopy of the BCAII-N_3^- system to reveal which motion of the protein is causing the observed frequency fluctuations.[36]

2D-IR spectroscopy has proven to be particularly suitable to detect underdamped low-frequency modes in proteins, as shown here and by Cheatum and co-workers using an IR probe (N_3^-) that happens to bind at the active site. However, to fully unravel the localization and scale of the observed motion(s), artificially introduced vibrational labels at positions distributed over the protein structure, for example, by using the *p*-cyanophenylalanine or the thiocyanate label, offer an elegant experimental strategy. Probing the environment in and around the active site may lead to a better understanding of the observed motion and may, furthermore, serve as benchmark for molecular dynamic simulations.

EXPERIMENTAL METHODS

Sample Preparation. CAII from bovine erythrocytes (*Bos taurus*) was purchased (Serva GmbH) and used without further purification. Identity and purity were confirmed by SDS-PAGE and nESI mass spectrometry (Figure S8). The BCAII (8 mM) N_3^- (6 mM) complex was prepared in 100 mM MES buffer at pH 7 (aqueous buffer). To prevent ice formation in low-temperature measurements, 66 wt % glycerol was added (cryogenic buffer). We placed 10 μL of the sample between CaF_2 windows separated by a 50 μm polytetrafluoroethylene spacer.

FTIR Spectroscopy. IR absorption spectra were collected on a Tensor 27 (Bruker) FTIR spectrometer with a HgCdTe (MCT) detector at a resolution of 1 cm^{-1}. The solvent background was fitted by a fifth-order polynomial excluding the region of N_3^- absorption (2040−2110 cm^{-1}) and subsequently subtracted.

CD Spectroscopy. Spectra were recorded on a J-720 (Jasco) CD spectrometer in the temperature range 293−363 K. For measurements in the near- and far-UV regions a sample thickness of 50 and 5 μm was used. The protein concentration was adjusted to 1.08 and 0.54 mM, respectively.

Mass Spectrometry. ESI-IMS-MS measurements of the protein in complex with N_3^- were performed on a Synapt G2-S instrument (Waters Corp., Manchester, UK) with a 32 kDa quadrupole in positive nESI mode. A capillary voltage of 1.8 kV was applied, the sample cone voltage was set at 100 V, and the source offset at 80 V. Data analysis was performed by using the software UniDec.[42]

Viscosity Modeling. The dynamic viscosity of the water−glycerol mixture (66 wt % glycerol) and pure water (see Figure S4) was modeled by using the Avramov−Milchev equation:[43,44]

https://doi.org/10.1021/acs.jpclett.1c01453
J. Phys. Chem. Lett. 2021, 12, 7777−7782

$$\eta(T) = \eta^0 \exp\left[(28.75 - \ln \eta^0)\left(\frac{T_g}{T}\right)^{\alpha}\right]$$

where η is the dynamic viscosity in cP, the initial viscosity η^0 = 0.364 cP, the glass temperature T_g = 168.64 K, and α = 3.74 in the case of the mixture.[44] For pure water η^0 = 0.112 cP, T_g = 141.0 K, and α = 3.2 were used.[44]

2D-IR Spectroscopy and CLS Analysis. A Ti:sapphire regenerative amplifier (2 mJ, 90 fs, 3 kHz repetition rate, Tsunami-Spitfire Ace combination, Spectra-Physics) system pumped two home-built optical parametric amplifiers (OPAs). Difference frequency generation in $AgGaS_2$ produced low-energy (<2 μJ) probe (and reference) pulses and high-energy (up to 10 μJ) pump pulses. The pump pulses were polarized perpendicular with respect to the probe pulses to reduce pump scatter. The pump pulse pair with adjustable delay was prepared by using a Michelson interferometer.[45] Fourier transform along this delay followed by phase correction yielded the purely absorptive 2D-IR spectrum.[45] The pump probe delay (T_w) was controlled by using an optical delay line. To suppress signals originating from pump scatter, phase cycling was performed by using an oscillating (f/4) ZnSe window at the Brewster angle.[46] Spectra were collected in 50 fs steps between 0 and 3 ps, in 0.5 ps steps up to 5 ps, and 1 ps steps up to 10 ps, where each spectrum contained (7−12) × 10^7 laser shots. A monochromator (300 lines/mm) dispersed the light onto a 2 × 64 pixel MCT array detector (Infrared Associates) for referenced detection. The liquid nitrogen level in the detector Dewar was maintained by an automated refilling system to facilitate continuous data acquisition.[47] The sample temperature was controlled to ±0.1 K by using a ST-100 cryostat (Janis).

The time-dependent line shape was analyzed by the inverse centerline slope (CLS) method.[37] For each time point the maximum in spectral cuts parallel to the ν_{pump} dimension of N_3^-'s 1−2 transition was determined. These points underwent linear regression yielding the centerline. Before FT, a linear fit of the CLS traces was subtracted, and the corrected data were multiplied by a tapered cosine window ($fraction_{cosine}$: 0.5; Figure 2, lower panel).

■ ASSOCIATED CONTENT

Supporting Information

The Supporting Information is available free of charge at https://pubs.acs.org/doi/10.1021/acs.jpclett.1c01453.

A figure displaying the X-ray crystal structure alignment of HCAII and BCAII,[30] exemplary 2D-IR spectra of N_3^- in BCAII between 0 and 5 ps, the dynamic viscosity of the water−glycerol mixture, CD and FTIR spectra of BCAII in aqueous and cryogenic buffer, temperature-dependent FTIR spectra of N_3^- in the range 232−323 K, vibrational lifetimes and the pure-dephasing time as a function of temperature of bound and free N_3^- in the protein sample, signal amplitudes of the 1−2 transition of bound N_3^- in the protein, nESI mass spectrometry results of BCAII and 2D-IR line shape analysis of N_3^- in BCAII by using the CLS and ivCLS technique on the 0−1 and 1−2 transition, respectively (PDF)

■ AUTHOR INFORMATION

Corresponding Author

Jens Bredenbeck − *Institute of Biophysics, Johann Wolfgang Goethe-University, 60438 Frankfurt am Main, Germany;* orcid.org/0000-0003-1929-9092; Email: bredenbeck@biophysik.uni-frankfurt.de

Authors

Julian M. Schmidt-Engler − *Institute of Biophysics, Johann Wolfgang Goethe-University, 60438 Frankfurt am Main, Germany;* orcid.org/0000-0002-4357-9943

Sarah von Berg − *Institute of Biophysics, Johann Wolfgang Goethe-University, 60438 Frankfurt am Main, Germany;* orcid.org/0000-0002-2855-3139

Complete contact information is available at: https://pubs.acs.org/10.1021/acs.jpclett.1c01453

Notes

The authors declare no competing financial interest.

■ ACKNOWLEDGMENTS

The authors thank the group of Prof. Nina Morgner for performing mass spectrometry. Furthermore, we thank the Deutsche Forschungsgemeinschaft for funding through INST 161/722-1 FUGG and the Alexander von Humboldt foundation for a Sofja Kovalevskaja award.

■ REFERENCES

(1) Wolfenden, R.; Snider, M. J. The Depth of Chemical Time and the Power of Enzymes as Catalysts. *Acc. Chem. Res.* **2001**, *34* (12), 938.

(2) Klinman, J. P. Dynamically achieved active site precision in enzyme catalysis. *Acc. Chem. Res.* **2015**, *48* (2), 449.

(3) Pauling, L. Nature of forces between large molecules of biological interest. *Nature* **1948**, *161* (4097), 707.

(4) Stojković, V.; Perissinotti, L. L.; Willmer, D.; Benkovic, S. J.; Kohen, A. Effects of the donor-acceptor distance and dynamics on hydride tunneling in the dihydrofolate reductase catalyzed reaction. *J. Am. Chem. Soc.* **2012**, *134* (3), 1738.

(5) Caratzoulas, S.; Mincer, J. S.; Schwartz, S. D. Identification of a protein-promoting vibration in the reaction catalyzed by horse liver alcohol dehydrogenase. *J. Am. Chem. Soc.* **2002**, *124* (13), 3270.

(6) Bhabha, G.; Biel, J. T.; Fraser, J. S. Keep on moving: discovering and perturbing the conformational dynamics of enzymes. *Acc. Chem. Res.* **2015**, *48* (2), 423.

(7) Benkovic, S. J.; Hammes-Schiffer, S. A perspective on enzyme catalysis. *Science* **2003**, *301* (5637), 1196.

(8) Hammes-Schiffer, S.; Benkovic, S. J. Relating protein motion to catalysis. *Annu. Rev. Biochem.* **2006**, *75*, 519.

(9) Schwartz, S. D. *Vibrationally Enhanced Tunneling from the Temperature Dependence of KIE, Isotope Effects in Chemistry and Biology*; CRC Press: Boca Raton, FL, 2006.

(10) Antoniou, D.; Basner, J.; Núñez, S.; Schwartz, S. D. Computational and theoretical methods to explore the relation between enzyme dynamics and catalysis. *Chem. Rev.* **2006**, *106* (8), 3170.

(11) Hay, S.; Scrutton, N. S. Good vibrations in enzyme-catalysed reactions. *Nat. Chem.* **2012**, *4* (3), 161.

(12) Nagel, Z. D.; Klinman, J. P. Tunneling and dynamics in enzymatic hydride transfer. *Chem. Rev.* **2006**, *106* (8), 3095.

(13) Wang, L.; Goodey, N. M.; Benkovic, S. J.; Kohen, A. Coordinated effects of distal mutations on environmentally coupled tunneling in dihydrofolate reductase. *Proc. Natl. Acad. Sci. U. S. A.* **2006**, *103* (43), 15753.

(14) Masgrau, L.; Roujeinikova, A.; Johannissen, L. O.; Hothi, P.; Basran, J.; Ranaghan, K. E.; Mulholland, A. J.; Sutcliffe, M. J.;

Scrutton, N. S.; Leys, D. Atomic description of an enzyme reaction dominated by proton tunneling. *Science* **2006**, *312* (5771), 237.
(15) Pineda, J. R. E. T.; Callender, R.; Schwartz, S. D. Ligand binding and protein dynamics in lactate dehydrogenase. *Biophys. J.* **2007**, *93* (5), 1474.
(16) Antoniou, D.; Schwartz, S. D. Internal Enzyme Motions as a Source of Catalytic Activity: Rate-Promoting Vibrations and Hydrogen Tunneling. *J. Phys. Chem. B* **2001**, *105* (23), 5553.
(17) Kohen, A. Role of dynamics in enzyme catalysis: substantial versus semantic controversies. *Acc. Chem. Res.* **2015**, *48* (2), 466.
(18) Warshel, A.; Bora, R. P. Perspective: Defining and quantifying the role of dynamics in enzyme catalysis. *J. Chem. Phys.* **2016**, *144* (18), 180901.
(19) Klinman, J. P.; Offenbacher, A. R.; Hu, S. Origins of Enzyme Catalysis: Experimental Findings for C-H Activation, New Models, and Their Relevance to Prevailing Theoretical Constructs. *J. Am. Chem. Soc.* **2017**, *139* (51), 18409.
(20) McGeagh, J. D.; Ranaghan, K. E.; Mulholland, A. J. Protein dynamics and enzyme catalysis: insights from simulations. *Biochim. Biophys. Acta, Proteins Proteomics* **2011**, *1814* (8), 1077.
(21) Schramm, V. L.; Schwartz, S. D. Promoting Vibrations and the Function of Enzymes. Emerging Theoretical and Experimental Convergence. *Biochemistry* **2018**, *57* (24), 3299.
(22) Smedarchina, Z.; Siebrand, W.; Fernández-Ramos, A.; Cui, Q. Kinetic isotope effects for concerted multiple proton transfer: a direct dynamics study of an active-site model of carbonic anhydrase II. *J. Am. Chem. Soc.* **2003**, *125* (1), 243.
(23) Christianson, D. W.; Fierke, C. A. Carbonic Anhydrase: Evolution of the Zinc Binding Site by Nature and by Design. *Acc. Chem. Res.* **1996**, *29* (7), 331.
(24) Lim, M.; Hamm, P.; Hochstrasser, R. M. Protein fluctuations are sensed by stimulated infrared echoes of the vibrations of carbon monoxide and azide probes. *Proc. Natl. Acad. Sci. U. S. A.* **1998**, *95* (26), 15315.
(25) Hill, S. E.; Bandaria, J. N.; Fox, M.; Vanderah, E.; Kohen, A.; Cheatum, C. M. Exploring the molecular origins of protein dynamics in the active site of human carbonic anhydrase II. *J. Phys. Chem. B* **2009**, *113* (33), 11505.
(26) Steiner, H.; Jonsson, B. H.; Lindskog, S. The catalytic mechanism of carbonic anhydrase. Hydrogen-isotope effects on the kinetic parameters of the human C isoenzyme. *Eur. J. Biochem.* **1975**, *59* (1), 253.
(27) Pocker, Y.; Bjorkquist, D. W. Comparative studies of bovine carbonic anhydrase in H_2O and D2O. Stopped-flow studies of the kinetics of interconversion of CO_2 and HCO3. *Biochemistry* **1977**, *16* (26), 5698.
(28) Venkatasubban, K. S.; Silverman, D. N. Carbon dioxide hydration activity of carbonic anhydrase in mixtures of water and deuterium oxide. *Biochemistry* **1980**, *19* (22), 4984.
(29) Jönsson, B. M.; Håkansson, K.; Liljas, A. The structure of human carbonic anhydrase II in complex with bromide and azide. *FEBS Lett.* **1993**, *322* (2), 186.
(30) Nguyen, M. N.; Tan, K. P.; Madhusudhan, M. S. CLICK–topology-independent comparison of biomolecular 3D structures. *Nucleic Acids Res.* **2011**, *39*, W24−8.
(31) Saito, R.; Sato, T.; Ikai, A.; Tanaka, N. Structure of bovine carbonic anhydrase II at 1.95 A resolution. *Acta Crystallogr., Sect. D: Biol. Crystallogr.* **2004**, *60*, 792.
(32) Pagano, P.; Guo, Q.; Kohen, A.; Cheatum, C. M. Oscillatory Enzyme Dynamics Revealed by Two-Dimensional Infrared Spectroscopy. *J. Phys. Chem. Lett.* **2016**, *7* (13), 2507.
(33) Pagano, P.; Guo, Q.; Ranasinghe, C.; Schroeder, E.; Robben, K.; Häse, F.; Ye, H.; Wickersham, K.; Aspuru-Guzik, A.; Major, D. T.; Gakhar, L.; Kohen, A.; Cheatum, C. M. Oscillatory Active-Site Motions Correlate with Kinetic Isotope Effects in Formate Dehydrogenase. *ACS Catal.* **2019**, *9*, 11199.
(34) Ranasinghe, C.; Pagano, P. L.; Sapienza, P. J.; Lee, A. L.; Kohen, A.; Cheatum, C. M. Isotopic Labeling of Formate Dehydrogenase Perturbs the Protein Dynamics. *J. Phys. Chem. B* **2019**, *123*, 10403.
(35) Adamczyk, K.; Simpson, N.; Greetham, G. M.; Gumiero, A.; Walsh, M. A.; Towrie, M.; Parker, A. W.; Hunt, N. T. Ultrafast infrared spectroscopy reveals water-mediated coherent dynamics in an enzyme active site. *Chem. Sci.* **2015**, *6* (1), 505.
(36) Baiz, C. R.; Błasiak, B.; Bredenbeck, J.; Cho, M.; Choi, J.-H.; Corcelli, S. A.; Dijkstra, A. G.; Feng, C.-J.; Garrett-Roe, S.; Ge, N.-H.; Hanson-Heine, M. W. D.; Hirst, J. D.; Jansen, T. L. C.; Kwac, K.; Kubarych, K. J.; Londergan, C. H.; Maekawa, H.; Reppert, M.; Saito, S.; Roy, S.; Skinner, J. L.; Stock, G.; Straub, J. E.; Thielges, M. C.; Tominaga, K.; Tokmakoff, A.; Torii, H.; Wang, L.; Webb, L. J.; Zanni, M. T. Vibrational Spectroscopic Map, Vibrational Spectroscopy, and Intermolecular Interaction. *Chem. Rev.* **2020**, *120* (15), 7152.
(37) Kwak, K.; Park, S.; Finkelstein, I. J.; Fayer, M. D. Frequency-frequency correlation functions and apodization in two-dimensional infrared vibrational echo spectroscopy: a new approach. *J. Chem. Phys.* **2007**, *127* (12), 124503.
(38) Guo, Q.; Pagano, P.; Li, Y.-L.; Kohen, A.; Cheatum, C. M. Line shape analysis of two-dimensional infrared spectra. *J. Chem. Phys.* **2015**, *142* (21), 212427.
(39) Elsaesser, T.; Huse, N.; Dreyer, J.; Dwyer, J. R.; Heyne, K.; Nibbering, E. T.J. Ultrafast vibrational dynamics and anharmonic couplings of hydrogen-bonded dimers in solution. *Chem. Phys.* **2007**, *341* (1−3), 175.
(40) Moritsugu, K.; Smith, J. C. Temperature-dependent protein dynamics: a simulation-based probabilistic diffusion-vibration Langevin description. *J. Phys. Chem. B* **2006**, *110* (11), 5807.
(41) Balog, E.; Becker, T.; Oettl, M.; Lechner, R.; Daniel, R.; Finney, J.; Smith, J. C. Direct determination of vibrational density of states change on ligand binding to a protein. *Phys. Rev. Lett.* **2004**, *93* (2), 28103.
(42) Marty, M. T.; Baldwin, A. J.; Marklund, E. G.; Hochberg, G. K. A.; Benesch, J. L. P.; Robinson, C. V. Bayesian deconvolution of mass and ion mobility spectra: from binary interactions to polydisperse ensembles. *Anal. Chem.* **2015**, *87* (8), 4370.
(43) Avramov, I. Viscosity in disordered media. *J. Non-Cryst. Solids* **2005**, *351* (40−42), 3163.
(44) Trejo González, J. A.; Longinotti, M. P.; Corti, H. R. The Viscosity of Glycerol−Water Mixtures Including the Supercooled Region. *J. Chem. Eng. Data* **2011**, *56* (4), 1397.
(45) Helbing, J.; Hamm, P. Compact implementation of Fourier transform two-dimensional IR spectroscopy without phase ambiguity. *J. Opt. Soc. Am. B* **2011**, *28* (1), 171.
(46) Bloem, R.; Garrett-Roe, S.; Strzalka, H.; Hamm, P.; Donaldson, P. Enhancing signal detection and completely eliminating scattering using quasi-phase-cycling in 2D IR experiments. *Opt. Express* **2010**, *18* (26), 27067.
(47) Deniz, E.; Eberl, K. B.; Bredenbeck, J. Note: An automatic liquid nitrogen refilling system for small (detector) Dewar vessels. *Rev. Sci. Instrum.* **2018**, *89* (11), 116101.

https://doi.org/10.1021/acs.jpclett.1c01453
J. Phys. Chem. Lett. 2021, 12, 7777−7782